21st International Conference on Pattern Recognition (ICPR 2012)
November 11-15, 2012. Tsukuba, Japan

Bone Suppression in Chest Radiographs by Means of Anatomically Specific Multiple Massive-Training ANNs

Sheng Chen[1,2] and Kenji Suzuki[2]
[1] *University of Shanghai for Science and Technology*
[2] *Department of Radiology, University of Chicago*
chnshn@hotmail.com; suzuki@uchicago.edu

Abstract

Our purpose was to separate bony structures such as ribs and clavicles from soft tissue in chest radiographs (CXRs). Although massive-training artificial neural networks (MTANNs) have been developed for suppression of ribs, they did not suppress rib edges, ribs close to the lung wall, and the clavicles well. To address this issue, we developed anatomically specific multiple MTANNs that are designed to suppress bones in different anatomic segments in the lungs. Each of 8 anatomically specific MTANNs was trained with the corresponding anatomic segment in the teaching bone images. The output segmental images from the 8 MTANNs were merged to produce a whole bone image. Total variation minimization smoothing was applied to the bone image for reduction of noise while edges were preserved;, then this bone image was subtracted from the original CXR to produce a soft-tissue image where bones are suppressed. We compared our new method with the conventional MTANNs by using a database of 110 CXRs with pulmonary nodules. Our anatomically specific MTANNs suppressed rib edges, ribs close to the lung wall, and the clavicles in CXRs substantially better than did the conventional MTANNs.

1. Introduction

Although chest radiography (CXR) is widely used for the detection of pulmonary nodules, the false-negative rate for nodules on CXRs is relatively high, and CXR is inferior to CT with respect to detectability of small nodules. Failure to detect nodules has been attributed to their size and density and to obscuring by structures such as ribs, clavicles, mediastinum, and pulmonary vessels. Studies have shown that up to 30% of nodules in CXRs could be missed by radiologists, and that 82%-95% of the missed nodules were partly obscured by overlying bones such as ribs and clavicles [1]. If such bony structures are suppressed in CXR, it would help radiologists improve their performance in lung nodule detection [2]. Suzuki et al. developed a supervised image-processing technique for suppressing ribs in CXRs by means of a multi-resolution MTANN [3-4]. Loog et al. proposed a supervised learning technique for suppression of ribs in CXRs [5]. The MTANN was able to suppress ribs in CXRs; however, rib edges, ribs close to the lung wall, and clavicles were not suppressed well.

Our purpose in this study was substantially to suppress bony structures such as rib edges, ribs close to the lung wall, and clavicles in CXRs. To achieve this goal, we developed anatomically specific multiple MTANNs, each of which was designed to process the corresponding anatomic segment in the lung field. We evaluated our new MTANNs by applying them to a test database of 110 CXRs with pulmonary nodules. We compared our new MTANNs with conventional MTANNs.

2. Method

2.1. Anatomically specific multiple MTANNs

An MTANN consists of a machine-learning regression model such as a linear-output artificial neural network (ANN) regression model that is capable of operating on pixel data directly [6]. The inputs to the MTANN are pixel values in a subregion, R, extracted from an input image. The output of the MTANN is a continuous scalar value, which is associated with the center pixel in the subregion, represented by

$$O(x,y) = ML\{I(x-i,y-j) \mid (i,j) \in R\}, \qquad (1)$$

where $ML(\cdot)$ is the output of the machine-learning regression model, and $I(x,y)$ is a pixel value of the

input image. For suppression of bones in CXRs, the MTANN is trained with input images and the corresponding "teaching" images. First, a CXR is divided pixel by pixel into a large number of overlapping subregions. Single pixels corresponding to the input subregions are extracted from the teaching images as teaching values. The error to be minimized by training of the MTANN is represented by

$$E = \frac{1}{P}\sum_{c}\sum_{(x,y)\in R_T}\left\{T_c(x,y) - O_c(x,y)\right\}^2, \qquad (2)$$

where c is the training case number, O_c is the output of the MTANN for the c^{th} case, T_c is the teaching value for the MTANN for the c^{th} case, and P is the number of total training pixels in the training region for the MTANN, R_T.

Although an MTANN was able to suppress ribs in CXRs[3-4], the single MTANN did not suppress rib edges, ribs close to the lung wall, and the clavicles well, because the orientation, width, contrast, and density of bones are different from location to location, and because the capability of a single MTANN is limited. To improve the suppression of bones at different locations, we extended the capability of a single MTANN and developed an anatomically specific multiple-MTANN scheme that consisted of 8 MTANNs arranged in parallel, as shown in Fig. 1a. Each anatomically specific MTANN was trained independently by use of normal cases and of nodule cases in which the nodules were located in the corresponding anatomic segment. We divided the lung field into 8 anatomic segments: a left upper segment for suppression of left clavicles and ribs, a left hilar segment for suppression of bone in the hilar area, a left middle segment for suppression of ribs in the middle of the lung field, a left lower segment for suppression of ribs in the left lower lobe, a right upper segment, a right hilar segment, a right middle segment, and a right lower segment. For each anatomically specific MTANN, the training samples were extracted specifically from the corresponding anatomic segment mask (the training region in Eq. 2).

After training, each of the segments in a non-training CXR was inputted to the corresponding trained anatomically specific MTANN for processing of the special anatomic segment in the lung field, e.g., MTANN no. 1 is trained to process the left-upper segment in the lung field in which clavicle lies; MTANN no. 2 is trained to process the left hilar segment, and so on, as illustrated in Fig. 1b. Then, the 8 segmental output subimages from the anatomically specific multiple MTANNs were composited to a whole bone image by use of the 8 anatomic segment masks which had been smoothed by a Gaussian filter to blend the subimages smoothly near their boundaries, represented by

$$f_b(x,y) = \sum_{i=1}^{8} O_i(x,y) \times f_G\left[M_i(x,y)\right], \qquad (3)$$

where $f_b(x,y)$ is the composite bone image, O_i is the i^{th} trained MTANN, $f_G(.)$ is a Gaussian filtering operator, and M_i is the i^{th} anatomic segmentation mask.

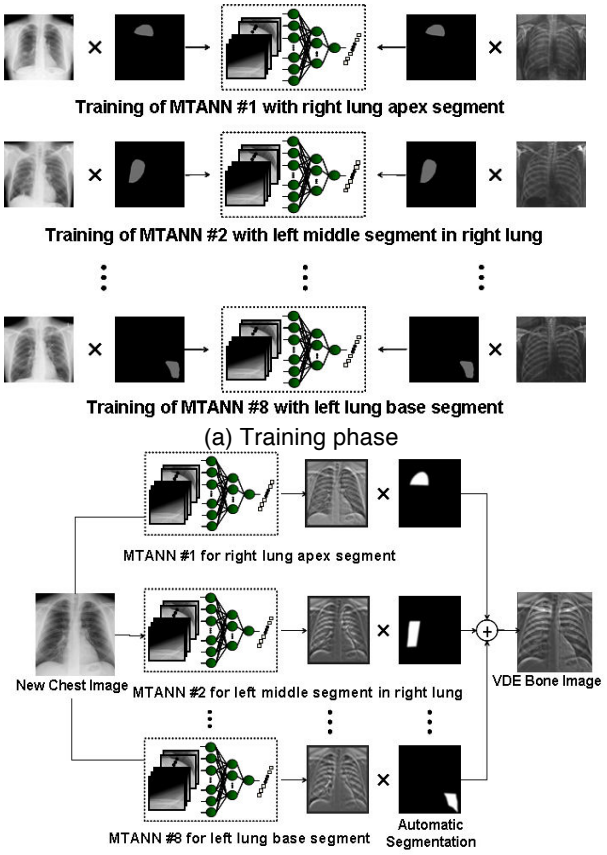

Figure 1. Architecture and training of our new anatomically specific MTANNs.

2.2. Training of anatomically specific MTANNs

To train 8 anatomically specific MTANNs, we used one normal CXR and 8 CXRs with nodules, each of which was located in a specific anatomic segment. Namely, we trained each MTANN with the normal case and the corresponding nodule case. We trained 8 MTANNs with input CXRs and the corresponding dual-energy bone images acquired with a dual-energy imaging system. For training of features in each anatomic segment in the lung field, 10,000 pairs of training samples were extracted randomly from the anatomic segment for each anatomically specific MTANN: 5,000 samples from the normal case, and

5,000 samples from the corresponding nodule case. We used a three-layered MTANN where the numbers of input, hidden, and output units were 81, 20, and 1, respectively. Once MTANNs were trained, the dual-energy imaging system was not necessary any more. The trained MTANNs are applicable to standard CXRs for suppression of bones; thus the term "virtual dual-energy" (VDE) technology. The advantages of this technology over real dual-energy imaging are that there is no need for special equipment to produce dual-energy images and no additional radiation dose to patients.

2.3. Automated anatomic segmentation

To determine the 8 anatomic segments, we developed an automated anatomic segmentation method based on active shape models (ASMs) [7]. First, we segmented the lung fields automatically by using our multi-segment ASM (M-ASM) scheme [8] which can be adapted to each of the segments of the lung boundaries (which we call a multi-segment adaptation approach), as illustrated in Fig. 2. Because the nodes in the conventional ASM are equally spaced along the entire lung shape, they do not fit lung shape parts with high curvatures. In our method, the model was improved by fixating of selected nodes at specific structural boundaries which we call transitional landmarks. Transitional landmarks identified the change from one boundary type (e.g., a boundary between the lung field and the heart) to another (e.g., a boundary between the lung field and the diaphragm). This resulted in multiple segmented lung-field boundaries where each segment is correlated with a specific boundary type (heart, aorta, rib cage, diaphragm, etc.). The node-specific ASM was built by using a fixed set of equally spaced nodes for each boundary segment. After the lungs were segmented, they were automatically divided into 8 anatomic segments by using the boundary types and of the transitional landmarks. By using the landmark points, we obtained the upper region, lower region, and hilar region in each lung, as illustrated in Fig. 2. We merged the 8 output segmental images from the multiple MTANNs into a single VDE bone image.

2.3 Creation of soft-tissue images

To reduce noise while preserving edges of bony structures in VDE bone images, we employed a total variation-minimization smoothing method. To create a VDE soft-tissue image, we subtracted the VDE bone image $f_b(x,y)$ from the corresponding original CXR $g(x,y)$ with a lung field mask image $m(x,y)$ as follows:

$$f_S(x,y) = g(x,y) - w_C \times f_b(x,y) \times m(x,y) \quad (4)$$

where w_C is a weighting parameter for determining the contrast of ribs.

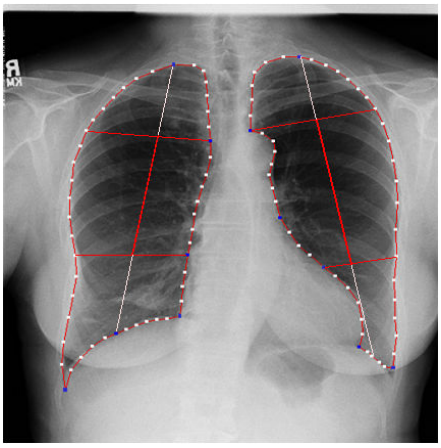

Figure 2. Result of automated anatomic segmentation based on our M-ASM.

3. Results

3.1. Database

The database used in our study consisted of 119 posterior-anterior CXRs acquired with a computed radiography (CR) system with a dual-energy subtraction unit (FCR 9501 ES; Fujifilm Medical Systems, Stamford, CT) at the University of Chicago Medical Center. The CXRs included 118 abnormal cases with pulmonary nodules and a "normal" case (i.e., a nodule-free case). Among them, 8 nodule cases and the normal case were used as a training set, and the rest were used as a test set. The matrix size of the CXRs was 1,760 x 1,760 pixels (pixel size: 0.2 mm; gray scale; 10 bits). Most nodules overlapped with ribs and/or clavicles in CXRs.

3.2 Evaluation

We applied our anatomically specific multiple MTANNs to a validation test set that included 110 nodule cases. Figure 3 illustrates the results of bone suppression. Compared to the old VDE soft-tissue images obtained by use of our conventional technique [4], rib edges, the clavicles, and ribs close to the lung wall are suppressed substantially, while the visibility of soft tissue such as lung nodules and vessels is maintained. The quality of the VDE soft-tissue images is comparable to that of the "gold-standard" dual-energy soft-tissue images. We evaluated the bone

suppression performance quantitatively by using the absolute error [4], represented by

$$E_N = \sum_{x,y \in R_L} |b(x,y) - f_b(x,y)| / N_L (b_{\max} - b_{\min}), \quad (5)$$

where $f_b(x,y)$ is the VDE bone image, $b(x,y)$ is the corresponding "gold-standard" dual-energy bone image, R_L indicates lung regions, N_L is the number of pixels in R_L, and b_{max} and b_{min} are the maximum value and the minimum value in R_L in the dual-energy bone image, respectively. The result for the 110 CXRs was an average E_N of 0.072 with a standard deviation of 0.012; both were smaller than our previous result [4] at a statistically significant level ($P<0.05$).

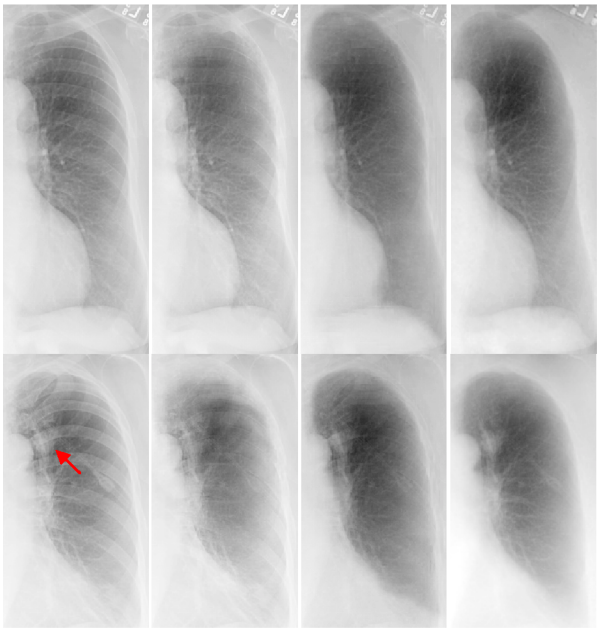

(a) (b) (c) (d)

Figure 3. Results of bone suppression for a normal case (upper) and a nodule case (lower; a nodule is indicated by an arrow). (a) Original CXRs. (b) Conventional VDE soft-tissue images. (c) New VDE soft-tissue images. (d) Corresponding "gold-standard" dual-energy soft-tissue images.

4. Conclusion

We have developed an anatomically specific multiple MTANN scheme to suppress bony structures in CXRs. With our new technique, rib edges, ribs close to the lung wall, and the clavicles were suppressed substantially better than was possible with our conventional technique, while soft tissue such as lung nodules and vessels was maintained. Thus, our technique would be useful for radiologists as well as for CADe schemes in the detection of lung nodules in CXRs.

5. Acknowledgement

This work was supported partially by NIH S10 RR021039 and P30 CA14599, and NSFC 81101116. Original bone suppression technology and source code have been non-exclusively licensed to Riverain Medical. It is the policy of University of Chicago that investigators disclose publicly actual or potential financial interests that may appear to be affected by research activities.

References

[1] P. K. Shah, J. H. Austin, C. S. White, P. Patel, L. B. Haramati, G. D. Pearson, M. C. Shiau, and Y. M. Berkmen, "Missed non-small cell lung cancer: radiographic findings of potentially resectable lesions evident only in retrospect," *Radiology,* vol. 226, pp. 235-241, Jan 2003.

[2] S. Oda, K. Awai, K. Suzuki, Y. Yanaga, Y. Funama, H. MacMahon, and Y. Yamashita, "Performance of radiologists in detection of small pulmonary nodules on chest radiographs: effect of rib suppression with a massive-training artificial neural network," *AJR. American Journal of Roentgenology,* vol. 193, pp. W397-402, Nov 2009.

[3] K. Suzuki, H. Abe, F. Li, and K. Doi, "Suppression of the contrast of ribs in chest radiographs by means of massive training artificial neural network," *Proc. SPIE Medical Imaing (SPIE MI),* vol. 5370, pp. 1109-1119, 2004.

[4] K. Suzuki, H. Abe, H. MacMahon, and K. Doi, "Image-processing technique for suppressing ribs in chest radiographs by means of massive training artificial neural network (MTANN)," *IEEE Transactions on Medical Imaging,* vol. 25, pp. 406-416, Apr 2006.

[5] M. Loog, B. van Ginneken, and A. M. Schilham, "Filter learning: application to suppression of bony structures from chest radiographs," *Med Image Anal,* vol. 10, pp. 826-840, Dec 2006.

[6] K. Suzuki, I. S. G. Armato, F. Li, S. Sone, and K. Doi, "Massive training artificial neural network (MTANN) for reduction of false positives in computerized detection of lung nodules in low-dose CT," *Medical Physics,* vol. 30, pp. 1602-1617, 2003.

[7] B. van Ginneken, M. B. Stegmann, and M. Loog, "Segmentation of anatomical structures in chest radiographs using supervised methods: a comparative study on a public database," *Med Image Anal,* vol. 10, pp. 19-40, Feb 2006.

[8] S. Chen, K. Suzuki, and H. MacMahon, "Development and evaluation of a computer-aided diagnostic scheme for lung nodule detection in chest radiographs by means of two-stage nodule enhancement with support vector classification," *Medical Physics,* vol. 38, pp.1844-1858, 2011.